Brief Communications

Prolonged Disynaptic Inhibition in the Cortex Mediated by Slow, Non-α7 Nicotinic Excitation of a Specific Subset of Cortical Interneurons

Sergio Arroyo,[1]* Corbett Bennett,[1]* David Aziz,[2] Solange P. Brown,[1,3] and Shaul Hestrin[1]

[1]Department of Comparative Medicine, Stanford University School of Medicine, Stanford, California 94305, [2]College of Optical Science, University of Arizona, Tucson, Arizona 85721, and [3]Department of Neuroscience, Johns Hopkins University School of Medicine, Baltimore, Maryland 21205

Cholinergic activation of nicotinic receptors in the cortex plays a critical role in arousal, attention, and learning. Here we demonstrate that cholinergic axons from the basal forebrain of mice excite a specific subset of cortical interneurons via a remarkably slow, non-α7 nicotinic receptor-mediated conductance. In turn, these inhibitory cells generate a delayed and prolonged wave of disynaptic inhibition in neighboring cortical neurons, altering the spatiotemporal pattern of inhibition in cortical circuits.

Introduction

The cholinergic system acts on both nicotinic and muscarinic receptors to facilitate numerous cognitive processes (Baxter and Chiba, 1999). Ascending axons from cholinergic neurons in the basal forebrain (BF) project throughout the cerebral cortex (Rye et al., 1984) where they provide the main source of cortical acetylcholine (ACh). Nicotinic acetylcholine receptors (nAChRs) have been shown to play an important role in attention (Howe et al., 2010; Guillem et al., 2011) and learning (Letzkus et al., 2011), and gain of function mutations in a non-α7 receptor subunit has been linked to a heritable form of epilepsy (Steinlein et al., 1995). Nicotinic receptors are prominently expressed on a subset of cortical interneurons (Porter et al., 1999; Christophe et al., 2002; Gulledge et al., 2007; Rudy et al., 2010), suggesting that cholinergic axon activation may modulate inhibition in the cortex. However, how endogenously released ACh affects the spatiotemporal pattern of cortical inhibition remains poorly understood.

To address this, we transduced cholinergic neurons in the BF with channelrhodopsin-2 (ChR2), allowing us to selectively stimulate cortical cholinergic afferents. We found that activation of cholinergic axons elicited a delayed and prolonged wave of inhibition in pyramidal cells and fast-spiking cells. Moreover, we demonstrate that this inhibitory barrage is generated by a strikingly slow non-α7 nicotinic receptor-mediated conductance in a subset of cortical interneurons.

Received Jan. 9, 2012; revised Feb. 3, 2012; accepted Feb. 8, 2012.

Author contributions: S.A., C.B., and S.H. designed research; S.A., C.B., and S.P.B. performed research; D.A. contributed unpublished reagents/analytic tools; S.A. and C.B. analyzed data; S.A., C.B., and S.H. wrote the paper.

We thank Rachel Hestrin and Pamelyn Woo for performing immunochemistry. We also thank Aaron Blankenship for contributing data. We thank Karl Deisseroth for help with viral transduction.

*S.A. and C.B. contributed equally to this work.

The authors declare no competing financial interests.

Correspondence should be addressed to Shaul Hestrin, 300 Pasteur Drive, Edwards R314, Department of Comparative Medicine, Stanford University School of Medicine, Stanford, CA 94305. E-mail: shaul.hestrin@stanford.edu.

DOI:10.1523/JNEUROSCI.0115-12.2012

 0270-6474/12/323859-06$15.00/0

Materials and Methods

Animals. Both a BAC transgenic (GENSAT GM24; Gong et al., 2007) and a knock-in mouse line (Rossi et al., 2011) expressing Cre recombinase (Cre) under the choline acetyltransferase (ChAT) promoter were used to transduce cholinergic neurons in the BF with a Cre-dependent ChR2-enhanced yellow fluorescent protein (ChR2-EYFP) construct. Both male and female mice were used for experiments. The expression of Cre in the BF was similar for both ChAT-Cre mouse lines (data not shown) and subsequent data were pooled. In addition, these animals were crossed with a Cre-dependent TdTomato reporter line (Jackson Laboratory 007905) to target ChAT-expressing bipolar (CB) interneurons and with a GAD67-GFP knock-in line (Δneo) to target late-spiking (LS) and fast-spiking (FS) interneurons (Tamamaki et al., 2003). All procedures were approved by the Administrative Panel on Laboratory Animal Care at Stanford University.

Viral transduction of the BF. Mice aged P20–P40 were anesthetized and placed in a stereotaxic frame. One to two microliters of adeno-associated virus (AAV)2/5 bearing a pAAV-EF1α-DIO-hChR2 (H134R)-EYFP-WPRE (Zhang et al., 2010) construct were pressure-injected into the brain using stereotaxic coordinates for several BF nuclei, including the nucleus basalis, the horizontal diagonal band of Broca, and the substantia innominata. Typically, four sites were injected, each with no more than 500 nL of virus.

Slice preparation. Six to eight weeks after surgery, each mouse was deeply anesthetized with isoflurane. Brains were removed in ice-cold, carbogenated sucrose composed of the following (in mM): 76 NaCl, 25 $NaHCO_3$, 25 glucose, 75 sucrose, 2.5 KCl, 1.75 $NaHPO_4$, 0.5 $CaCl_2$, 7 $MgSO_4$, 2 pyruvic acid, 4 lactic acid, 4 β-hydroxybutyric acid. Sagittal slices (300 μm thick) were generated (Integraslice 7550 MM, Campden Instruments) and transferred to a chamber with the same solution maintained at 32–35°C. After 30 min the slices were transferred to artificial CSF (ACSF) composed of the following (in mM): 125 NaCl, 2.5 KCl, 1.25 NaH_2PO_4, 1 $MgSO_4$, 2 $CaCl_2$, 26 $NaHCO_3$, 20 glucose, 4 lactic acid, 2 pyruvic acid, 0.4 ascorbic acid, and 4 β-hydroxybutyric acid at 32–35°C. However, in experiments examining disynaptic inhibition, 3.5 mM KCl ACSF was used. Slices were allowed to equilibrate to room temperature before being transferred to the microscope chamber.

Electrophysiological recordings. Glass electrodes (2–5 MΩ) were filled with an internal solution composed of the following (in mM): 2.7 KCl, 120 potassium methylsulfate, 9 HEPES, 0.18 EGTA, 4 MgATP, 0.3

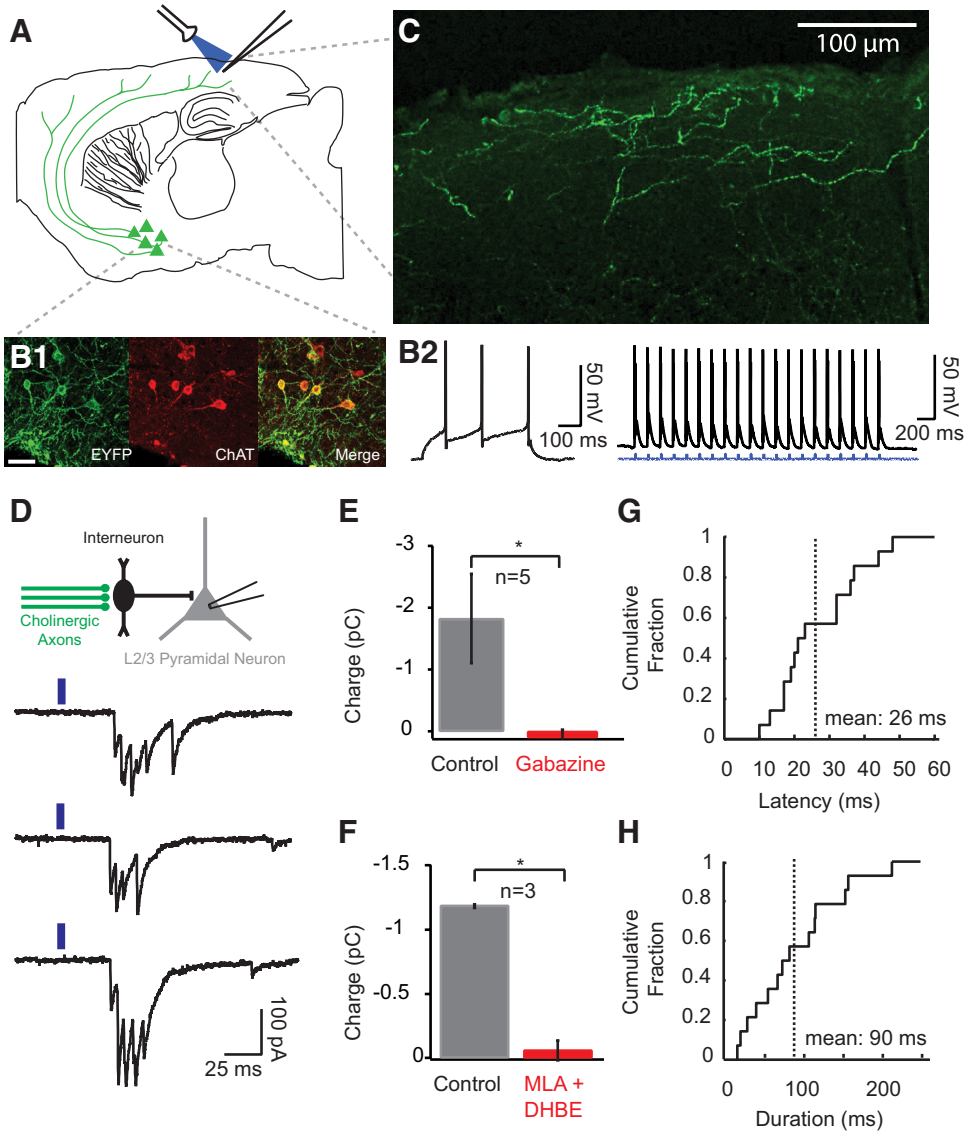

Figure 1. Nicotinic receptor-dependent inhibitory barrage in L2/3 pyramidal cells. ***A***, Experimental setup: The BF of ChAT-Cre mice was injected with an AAV vector driving Cre-dependent ChR2-EYFP expression in ChAT-expressing cells (green somas and fibers). ***B1***, EYFP (left) and ChAT immunostaining (middle) colocalize (right), indicating selective transduction of ChAT-expressing cells. Scale bar, 50 μm. ***B2***, Whole-cell recording from a virally transduced TdTomato labeled cell in the BF of a ChAT-Cre/TdTomato mouse. Left, Action potentials evoked during a step current injection; Right, A train of brief photostimulations (3 ms flashes at 6.7 Hz) evoked a train of action potentials in the cell. ***C***, Confocal image showing ChR2-EYFP-expressing axons in cortex. ***D***, Top, Diagram illustrating disynaptic inhibition generated by cholinergic axons; Bottom, Brief photostimulation (blue bar) evokes a barrage of PSCs in a L2/3 pyramid over multiple trials. Recordings were performed in DNQX (5 μM) with a high chloride internal solution (130 mM). ***E***, Bath application of gabazine (10 μM) abolished the photostimulation-induced barrage; $*p = 0.048$, paired *t* test. ***F***, Bath application of the nicotinic receptor antagonists MLA (5 nM) and DHβE (500 nM) abolished the photostimulation-induced barrage; $*p = 0.005$, paired *t* test. ***G***, Cumulative incidence of barrage latencies for 14 L2/3 pyramidal cells. Latencies were computed for each cell from an average of several trials. ***H***, Cumulative incidence of barrage duration for same cells as in ***G***.

NaGTP, and 20 sodium phosphocreatine; pH 7.3, 295 mOsm/L. Whole-cell patch-clamp recordings were obtained at room temperature using two Axopatch 200B or 700A patch amplifiers (Molecular Devices) in current-clamp or voltage-clamp modes. Data acquisition and offline analysis were performed using custom software written in IGOR Pro (Wavemetrics). For photostimulation, blue light was emitted either from an LED attached to a fiber-optic cable (920 μm diameter) or a xenon lamp with a mechanical shutter (Uniblitz, Vincent Associates). The spot used to illuminate the slice ranged from 200 to 450 μm in diameter and the light intensity ranged from 10 to 400 mW/mm^2. Photostimulation was typically 3–5 ms long, and 2–5 min were allowed between stimulations. In a small fraction of experiments, photostimulation was up to 10 ms due to the mechanics of the shutter. However, no difference in the response kinetics was observed for these data, and thus all of the data were pooled. L1 cells were recorded in all animals to verify transduction and expression of ChR2. For pharmacological experiments, tetrodotoxin (TTX), 6,7-dinitroquinoxaline-2,3-dione (DNQX), methyllycaconitine (MLA), and dihydro-β-erythroidine (DHβE) were diluted in ACSF to 0.5 μM, 10 μM, 5 nM, and 500 nM, respectively, and bath applied.

Identification of interneuron subtypes. L1 neurons were identified by laminar position within the cortex. Layer 2/3 LS and FS cells were identified by fluorescence in Δneo animals and by response to current injection. However, the FS cells recorded in Figure 3 (see Results) were identified by morphology under DIC and electrophysiological characteristics alone. LS cells displayed a slow depolarizing ramp during current injection and a delayed action potential at threshold. FS cells displayed a discharge firing pattern near threshold, a relatively small degree of interspike interval (ISI) variability (ISI coefficient of variability = 0.13 ± 0.1, n = 6 cells), and a low input resistance (123 ± 69 MΩ) as described previously (Kawaguchi, 1995). CB interneurons were identified by fluorescence in a ChAT-Cre/tdTomato reporter line. Neurons with bipolar morphology that expressed tdTomato were targeted for recording and

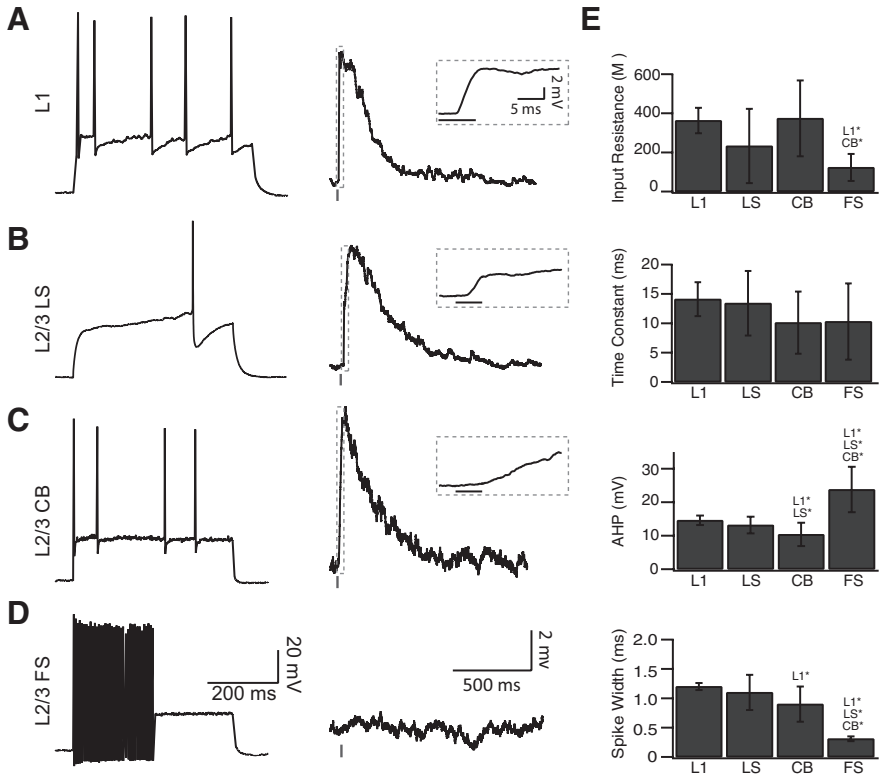

Figure 2. Responses to cholinergic fiber stimulation in four types of interneurons in layer 1 and layer 2/3. ***A***, Characteristic firing pattern of a layer 1 (L1) interneuron in response to current injection (left) and a representative response of the same cell to photostimulation of cholinergic fibers (tick mark below trace; right). The dotted boundary indicates the region expanded in the inset (upper right). Inset scale bar applies to all insets below. Black lines in all insets represent photostimulation. ***B***, Same as ***A***, but for a L2/3 LS cell. ***C***, Same as ***A***, but for a L2/3 CB cell. ***D***, Same as ***A***, but for a L2/3 FS cell. Scale bars apply to traces above. ***E***, Input resistance, time constant, AHP, and spike width are plotted for L1, L2/3 LS cells, L2/3 CB, and L2/3 FS cells; $*p < 0.05$, paired *t* test.

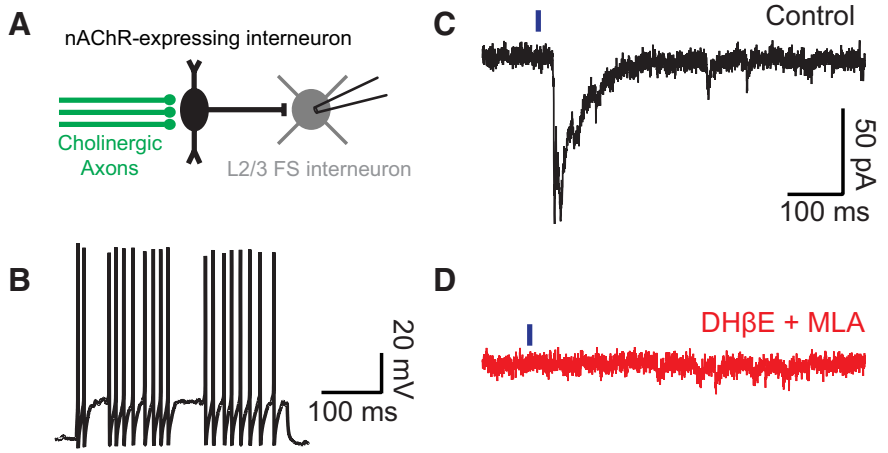

Figure 3. Inhibitory barrage in layer 2/3 fast-spiking cells. ***A***, Diagram illustrating disynaptic inhibition in FS interneurons generated by cholinergic axons. ***B***, Action potentials evoked in response to current injection for an FS cell. ***C***, Photostimulation evoked an IPSC barrage in this cell. ***D***, The photostimulation-evoked IPSC barrage is abolished by DHβE (500 nM) together with MLA (5 nM).

displayed irregular spiking during step current injections (see Fig. 2*C*). Spike threshold was defined by an empirical criterion described previously (Azouz and Gray, 2000). Electrophysiological parameters for all cell types are summarized in Figure 2.

Analysis. Response kinetics were determined from voltage-clamp recordings to separate the fast and slow components. All voltage-clamp recordings used for analysis were performed in DNQX (10 μM). Rise times were defined as the time from 20 to 80% of the peak response. For cells with both fast and slow components, the slow component rise time was analyzed after application of MLA (5 nM). Decay τs were estimated by fitting single exponential functions to each trace. To calculate the charge transferred by an inhibitory postsynaptic current (IPSC) barrage, traces were integrated between 0 and 200 ms after photostimulation. To calculate the latency of the barrage, traces were binned into 1 ms intervals and the latency was defined as the first bin after photostimulation to exceed 3 SDs above the mean of the baseline before photostimulation. To compute the duration of the barrage, the total charge transferred was calculated by integrating the trace between 0 and 1000 ms after photostimulation. The duration was defined as the time required to transfer 20–80% of this total charge. All values are reported as the mean ± SE unless otherwise indicated. A paired *t* test was used for all statistical comparisons except for cases in which the Lilliefors test rejected the null hypothesis that the samples represented a normal distribution. In these cases, the Wilcoxon rank sum test was used.

Immunohistochemistry and confocal imaging. Images of EYFP-labeled processes were taken of tissue after electrophysiological recordings. The slice was fixed in 4% paraformaldehyde and mounted in VectaShield. Images were acquired on a Zeiss LSM Pascal confocal microscope. For immunohistochemistry, the whole brain was dissected and fixed in 4% paraformaldehyde for 2 h. After rinses in 0.01 M PBS, 30 μm thick sections were prepared and mounted on slides. The tissue was then permeabilized in 0.4% Triton, blocked with 3% donkey serum, and incubated in goat anti-ChAT (Millipore) overnight at 4°C. The following day, the tissue was rinsed three times in PBS and incubated in the appropriate secondary (donkey anti-goat) conjugated to an Alexa fluorophore for 2 h at room temperature. Finally, the tissue was rinsed three times in PBS, mounted in VectaShield, and confocal images were acquired with a 20× (air) or 63× (oil-immersion) objective lens.

Results

We began by asking whether activation of cholinergic axons could trigger action potentials in nicotinic receptor-expressing interneurons and generate disynaptic inhibition in neighboring cortical neurons. To selectively activate BF cholinergic inputs, we injected an AAV viral vector bearing the construct for a Cre-dependent ChR2-EYFP fusion protein into the BF in two mouse lines expressing Cre under the ChAT promoter (Gong et al., 2007; Rossi et al., 2011). Immunohistochemistry and electrophysiological recordings revealed that ChAT cells in the BF were selectively transduced with ChR2-EYFP and could be activated with brief flashes of blue light (Fig. 1*B*). We obtained whole-cell patch-clamp recordings from layer 2/3 (L2/3) pyramidal cells in sensorimotor cortex and photostimulated ChR2-expressing cholinergic fibers (Fig. 1*A*,*C*). To facilitate detection of IPSCs, we included a high

chloride (130 mM) solution in the recording pipette and the slices were bathed in physiological K^+ (3.5 mM). DNQX (5 μM) was bath-applied to block AMPAR-mediated glutamatergic transmission. Under these conditions, brief photostimulation (3–5 ms) evoked a delayed barrage of IPSCs in L2/3 pyramidal cells (15/40; Fig. 1*D*). This barrage was abolished by the $GABA_A$-receptor antagonist gabazine ($n = 5$; $p = 0.048$; *t* test; Fig. 1*E*) and by nicotinic receptor blockade with DHβE (500 nM) together with MLA (5 nM; $n = 3$; *t* test; $p = 0.005$; Fig. 1*F*). These results indicate that cholinergic fibers activate nicotinic receptors to generate disynaptic feedforward inhibition in pyramidal cells.

The inhibitory barrage in L2/3 pyramidal cells exhibited a long latency (mean latency: 26 ms; Fig. 1*G*) and duration (mean duration: 90 ms; Fig. 1*H*). How can the brief activation of cholinergic afferents produce a delayed and prolonged wave of inhibition? To answer this question, we recorded responses to photostimulation from four classes of cortical interneurons. Photostimulation evoked EPSPs in layer 1 (L1) cells (77/77), L2/3 LS cells (12/12), and L2/3 CB cells (14/14; Fig. 2). In contrast, FS cells did not exhibit EPSPs (0/7; Fig. 2*D*), but instead received an inhibitory barrage similar to the responses observed in pyramidal neurons ($n = 2$; Fig. 3). Photostimulation-evoked EPSPs were abolished by TTX (500 nM; $n = 4$, $p = 0.03$; *t* test) and by MLA/DHβE ($n = 4$, $p = 0.03$; rank sum test; Fig. 4*A*), indicating that they were action potential-dependent and nicotinic receptor-mediated.

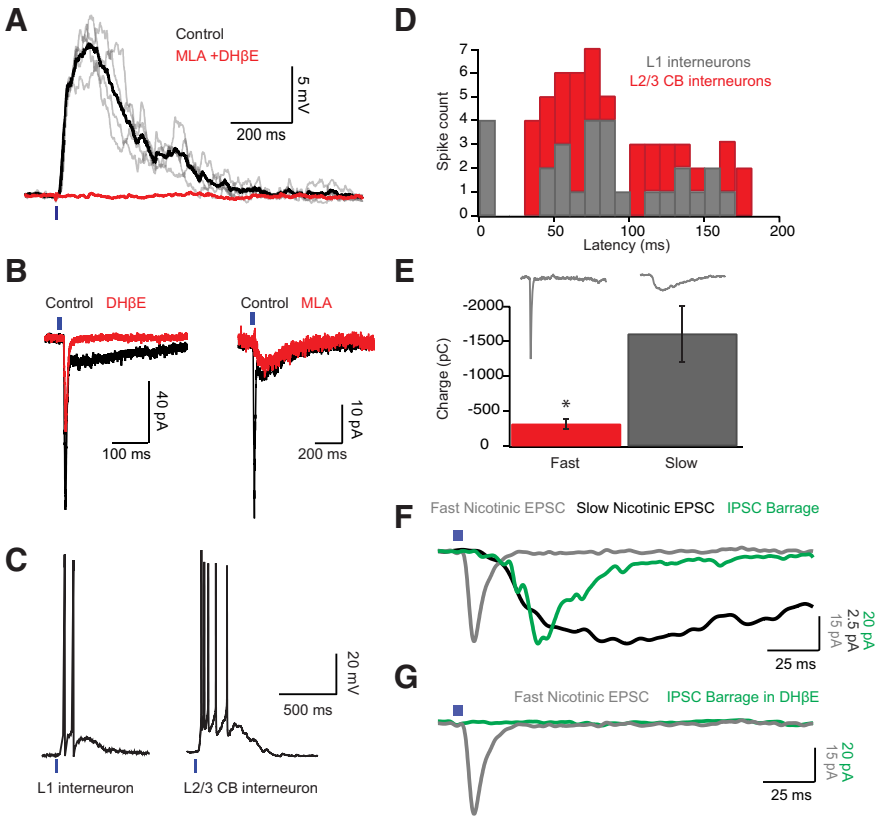

Figure 4. Cholinergic axons elicit a prolonged nicotinic excitation in cortical interneurons. ***A***, Response of a L1 cell to brief (3 ms) photostimulation in control conditions (black) and in 5 nM MLA and 500 nM DHβE (red). Superimposed gray traces represent single trial responses. ***B***, Voltage-clamp recordings from two L1 interneurons reveals two nicotinic receptor-mediated components. Application of 500 nM DHβE, a non-α7 nicotinic receptor antagonist, selectively blocks the slow EPSC (left, control in black). In contrast, the selective α7 receptor antagonist MLA (5 nM) abolishes the fast component (right, control in black). ***C***, Photostimulation-evoked bursts of action potentials in a L1 cell and a L2/3 CB cell. ***D***, Spike latency histogram for all spiking L1 and L2/3 CB cells. Counts for each cell type are stacked. ***E***, Charge transferred by the pharmacologically isolated fast and slow EPSCs. Traces above the bar graph depict the population-averaged waveforms of the fast ($n = 6$) and slow ($n = 4$) EPSCs; *$p = 0.005$, *t* test. ***F***, The time course of the averaged IPSC barrage recorded in pyramidal cells ($n = 4$ cells, green) is superimposed on the averaged fast EPSC (isolated with DHβE; $n = 6$ cells, light gray) and slow EPSC (isolated with MLA; $n = 4$ cells, dark gray) for comparison. ***G***, Application of DHβE spares the fast component of the nicotinic EPSC but abolishes the slow nicotinic EPSC and the IPSC barrage ($n = 3$).

Strikingly, the evoked excitatory responses in all L1, LS, and CB cells tested displayed remarkably slow decay kinetics (decay τ for L1: 176 ± 10 ms, $n = 33$; L2/3 LS: 215 ± 14 ms, $n = 12$; L2/3 CB: 234 ± 19 ms, $n = 14$). The EPSP decay time constant was an order of magnitude greater than the membrane time constants for L1, LS, and CB cells (Fig. 2*E*), suggesting that the response kinetics reflect the waveform of the underlying nicotinic conductance. Indeed, voltage-clamp recordings revealed a slow current in all L1 cells ($n = 11/11$; rise time: 35 ± 5 ms; decay τ: 190 ± 17 ms) and L2/3 CB cells tested ($n = 5/5$; rise time: 14 ± 1 ms; decay τ: 218 ± 16 ms). Interestingly, DHβE (500 nM) abolished this slow EPSC, indicating that it was mediated exclusively by non-α7 nAChRs (Fig. 4*B*, left). In addition to this slow current, a subset of L1 cells ($n = 6/11$) exhibited a fast EPSC (rise time: 2.6 ± 0.5 ms; decay τ of 4.9 ± 0.6 ms) that was abolished by the selective α7 receptor antagonist MLA (5 nM; Fig. 4*B*, right). Indeed, close inspection of current-clamp traces from L1 (17/40) and L2/3 LS (5/12) cells, but not CB cells (0/14), revealed a fast component manifesting as a notch in the rise of the EPSP (Fig. 2*A–C*) that was abolished by MLA (5 nM).

Do these two nAChR subtypes contribute differentially to the IPSC barrage observed in pyramidal cells? Photostimulation of cholinergic fibers produced action potentials in postsynaptic interneurons (8 cells total; 4 L1 cells and 4 CB cells). In 5 of 8 of these cells, single nicotinic EPSPs elicited bursts of action potentials ($n = 2/4$ L1 cells; $n = 3/4$ CB cells; Fig. 4*C*). The majority of evoked action potentials occurred after a latency of 30–180 ms (Fig. 4*D*), indicating that they were likely mediated by the slow non-α7 EPSP. Consistent with this hypothesis, we found that the charge associated with the slow non-α7 receptor-mediated EPSC was fivefold larger than that associated with the fast α7 EPSC (slow: 1610 ± 404 pC; fast: 315 ± 79 pC; $p = 0.005$; *t* test; Fig. 4*E*). Moreover, comparison of the time course of the IPSC barrage and the two nicotinic EPSCs indicates that the disynaptic inhibition is predominantly produced during the slow EPSC (Fig. 4*F*). Indeed, application of DHβE (500 nM) abolished the inhibitory barrage ($n = 3/3$ pyramidal cells; Fig. 4*G*) but spared the fast, α7 receptor-mediated input.

Discussion

Although the cholinergic system is critical to cognition, strikingly little is known about the mechanisms by which endogenously released ACh modulates cortical activity. We found that activation of BF fibers produced cell type-specific responses in cortical interneurons. L1 cells and L2/3 LS cells exhibited both a fast and a slow response, while L2/3 ChAT bipolar cells exhibited only a

slow response. We demonstrate that the fast and slow components are mediated α7 receptors and non-α7 receptors, respectively. Finally, we show that non-α7 receptor-mediated excitation elicits action potentials in cortical interneurons to produce a delayed and prolonged wave of inhibition in L2/3 pyramidal neurons and FS cells.

Dual-component nicotinic responses

Activation of cholinergic axons elicits slow, non-α7 nicotinic receptor-mediated responses in L1, L2/3 LS, and L2/3 CB cells. Due to their slow kinetics and large charge transfer, these EPSPs are capable of producing bursts of action potentials in non-α7 receptor-expressing cells. In addition to this slow response, a subset of nAChR-expressing cells (L1 and L2/3 LS cells) also exhibited a fast, α7 nicotinic receptor-mediated EPSC similar to responses observed in the hippocampus (Alkondon et al., 1998; Frazier et al., 1998). Although α7-mediated excitation does not appear to generate disynaptic inhibition under our experimental conditions, it should be noted that α7 responses may drive spikes more readily *in vivo* due to increased background activity. Moreover, given their high Ca^{2+} permeability (Dani and Bertrand, 2007), α7 receptors may play an important role in intracellular signaling and plasticity (Gu and Yakel, 2011).

The remarkably slow time course of the non-α7 response suggests that it may be mediated by a different synaptic mechanism than the fast α7 response. Indeed, it has been proposed that cholinergic signaling in the cortex operates by both volume transmission and conventional synaptic transmission (Umbriaco et al., 1994; Smiley et al., 1997; Turrini et al., 2001; Sarter et al., 2009). Further studies are needed to determine whether the slow kinetics of the non-α7 response reflects intrinsic channel kinetics or the diffusion of acetylcholine through extracellular space.

Cell-type specificity

We find that endogenously released acetylcholine elicits nicotinic receptor-mediated responses in specific interneuron subtypes (L1, LS, CB) but not others (FS). The specificity of BF outputs suggests that these interneuron classes contribute to the cognitive processes typically associated with the BF including attention, learning, and memory. Indeed, cortical ChAT/VIP interneurons have been shown to dilate local microvasculature, thus providing increased blood supply during periods of elevated activity (Cauli et al., 2004; Kocharyan et al., 2008). In this way, the BF may help supply the increased metabolic demands associated with attention and memory in specific cortical regions (Corbetta et al., 1991; Blaizot et al., 2000). Moreover, the fast nicotinic receptor-mediated recruitment of specific classes of interneurons (L1 and LS) may help to synchronize cortical activity and initiate oscillations, a phenomenon widely associated with attention and synaptic plasticity (Ji and Dani, 2000). Indeed, LS cells are connected to each other and various other interneuron types via an extensive network of gap junctions (Simon et al., 2005), and are thus well suited for synchronization of cortical circuits.

Spatiotemporal pattern of inhibition

In a recent study, Letzkus et al. (2011) suggested that cholinergic activation of cortical interneurons after a foot shock leads to disynaptic inhibition of FS cells and consequently to disinhibition of pyramidal neurons. Consistent with this report, we find that FS cells do not exhibit direct nicotinic responses, but instead receive a barrage of IPSCs in response to cholinergic activation. However, we also find that pyramidal cells themselves receive disynaptic nicotinic receptor-mediated inhibition. There are at least two possible explanations for this discrepancy. First, FS cells are generally not active in acute slices. Thus, under our experimental conditions, inhibition of FS cells will not produce disinhibition of pyramidal cells. Second, whereas our preparation allows us to recruit all ascending cholinergic axons, aversive shocks may activate a specific subset of these fibers which do not drive disynaptic inhibition in pyramidal cells.

Interestingly, FS cells inhibit inputs onto the soma and proximal dendrites of pyramidal neurons, while nicotinic receptor-expressing interneurons are thought to preferentially target distal dendrites (Kawaguchi and Kubota, 1997). Thus, by activating specific classes of interneurons and suppressing others, the BF may dynamically shape the pattern of inhibition imposed on cortical circuits (Xiang et al., 1998). Moreover we propose that, given the delayed kinetics of the IPSC barrage, sensory activation of the BF will preferentially impact long latency intracortical activity over the initial feedforward sensory response (Lamme and Roelfsema, 2000). Thus, the prolonged disynaptic inhibition we observe here may facilitate attention and arousal by favoring the processing of external inputs over intracortical interactions.

References

Alkondon M, Pereira EF, Albuquerque EX (1998) alpha-bungarotoxin- and methyllycaconitine-sensitive nicotinic receptors mediate fast synaptic transmission in interneurons of rat hippocampal slices. Brain Res 810:257–263.

Azouz R, Gray CM (2000) Dynamic spike threshold reveals a mechanism for synaptic coincidence detection in cortical neurons in vivo. Proc Natl Acad Sci U S A 97:8110–8115.

Baxter MG, Chiba AA (1999) Cognitive functions of the basal forebrain. Curr Opin Neurobiol 9:178–183.

Blaizot X, Landeau B, Baron JC, Chavoix C (2000) Mapping the visual recognition memory network with PET in the behaving baboon. J Cereb Blood Flow Metab 20:213–219.

Cauli B, Tong XK, Rancillac A, Serluca N, Lambolez B, Rossier J, Hamel E (2004) Cortical GABA interneurons in neurovascular coupling: relays for subcortical vasoactive pathways. J Neurosci 24:8940–8949.

Christophe E, Roebuck A, Staiger JF, Lavery DJ, Charpak S, Audinat E (2002) Two types of nicotinic receptors mediate an excitation of neocortical layer I interneurons. J Neurophysiol 88:1318–1327.

Corbetta M, Miezin FM, Dobmeyer S, Shulman GL, Petersen SE (1991) Selective and divided attention during visual discriminations of shape, color, and speed: functional anatomy by positron emission tomography. J Neurosci 11:2383–2402.

Dani JA, Bertrand D (2007) Nicotinic acetylcholine receptors and nicotinic cholinergic mechanisms of the central nervous system. Annu Rev Pharmacol Toxicol 47:699–729.

Frazier CJ, Rollins YD, Breese CR, Leonard S, Freedman R, Dunwiddie TV (1998) Acetylcholine activates an alpha-bungarotoxin-sensitive nicotinic current in rat hippocampal interneurons, but not pyramidal cells. J Neurosci 18:1187–1195.

Gong S, Doughty M, Harbaugh CR, Cummins A, Hatten ME, Heintz N, Gerfen CR (2007) Targeting Cre recombinase to specific neuron populations with bacterial artificial chromosome constructs. J Neurosci 27:9817–9823.

Gu Z, Yakel JL (2011) Timing-dependent septal cholinergic induction of dynamic hippocampal synaptic plasticity. Neuron 71:155–165.

Guillem K, Bloem B, Poorthuis RB, Loos M, Smit AB, Maskos U, Spijker S, Mansvelder HD (2011) Nicotinic acetylcholine receptor beta2 subunits in the medial prefrontal cortex control attention. Science 333:888–891.

Gulledge AT, Park SB, Kawaguchi Y, Stuart GJ (2007) Heterogeneity of phasic cholinergic signaling in neocortical neurons. J Neurophysiol 97:2215–2229.

Howe WM, Ji J, Parikh V, Williams S, Mocaër E, Trocmé-Thibierge C, Sarter M (2010) Enhancement of attentional performance by selective stimulation of alpha4beta2(*) nAChRs: underlying cholinergic mechanisms. Neuropsychopharmacology 35:1391–1401.

Ji D, Dani JA (2000) Inhibition and disinhibition of pyramidal neurons by activation of nicotinic receptors on hippocampal interneurons. J Neurophysiol 83:2682–2690.

Kawaguchi Y (1995) Physiological subgroups of nonpyramidal cells with specific morphological characteristics in layer II/III of rat frontal cortex. J Neurosci 15:2638–2655.

Kawaguchi Y, Kubota Y (1997) GABAergic cell subtypes and their synaptic connections in rat frontal cortex. Cereb Cortex 7:476–486.

Kocharyan A, Fernandes P, Tong XK, Vaucher E, Hamel E (2008) Specific subtypes of cortical GABA interneurons contribute to the neurovascular coupling response to basal forebrain stimulation. J Cereb Blood Flow Metab 28:221–231.

Lamme VA, Roelfsema PR (2000) The distinct modes of vision offered by feedforward and recurrent processing. Trends Neurosci 23:571–579.

Letzkus JJ, Wolff SB, Meyer EM, Tovote P, Courtin J, Herry C, Lüthi A (2011) A disinhibitory microcircuit for associative fear learning in the auditory cortex. Nature 480:331–335.

Porter JT, Cauli B, Tsuzuki K, Lambolez B, Rossier J, Audinat E (1999) Selective excitation of subtypes of neocortical interneurons by nicotinic receptors. J Neurosci 19:5228–5235.

Rossi J, Balthasar N, Olson D, Scott M, Berglund E, Lee CE, Choi MJ, Lauzon D, Lowell BB, Elmquist JK (2011) Melanocortin-4 receptors expressed by cholinergic neurons regulate energy balance and glucose homeostasis. Cell Metab 13:195–204.

Rudy B, Fishell G, Lee S, Hjerling-Leffler J (2011) Three groups of interneurons account for nearly 100% of neocortical GABAergic neurons. Dev Neurobiol 71:45–61.

Rye DB, Wainer BH, Mesulam MM, Mufson EJ, Saper CB (1984) Cortical projections arising from the basal forebrain: a study of cholinergic and noncholinergic components employing combined retrograde tracing and immunohistochemical localization of choline acetyltransferase. Neuroscience 13:627–643.

Sarter M, Parikh V, Howe WM (2009) Phasic acetylcholine release and the volume transmission hypothesis: time to move on. Nat Rev Neurosci 10:383–390.

Simon A, Oláh S, Molnár G, Szabadics J, Tamás G (2005) Gap-junctional coupling between neurogliaform cells and various interneuron types in the neocortex. J Neurosci 25:6278–6285.

Smiley JF, Morrell F, Mesulam MM (1997) Cholinergic synapses in human cerebral cortex: an ultrastructural study in serial sections. Exp Neurol 144:361–368.

Steinlein OK, Mulley JC, Propping P, Wallace RH, Phillips HA, Sutherland GR, Scheffer IE, Berkovic SF (1995) A missense mutation in the neuronal nicotinic acetylcholine receptor alpha 4 subunit is associated with autosomal dominant nocturnal frontal lobe epilepsy. Nat Genet 11:201–203.

Tamamaki N, Yanagawa Y, Tomioka R, Miyazaki J, Obata K, Kaneko T (2003) Green fluorescent protein expression and colocalization with calretinin, parvalbumin, and somatostatin in the GAD67-GFP knock-in mouse. J Comp Neurol 467:60–79.

Turrini P, Casu MA, Wong TP, De Koninck Y, Ribeiro-da-Silva A, Cuello AC (2001) Cholinergic nerve terminals establish classical synapses in the rat cerebral cortex: synaptic pattern and age-related atrophy. Neuroscience 105:277–285.

Umbriaco D, Watkins KC, Descarries L, Cozzari C, Hartman BK (1994) Ultrastructural and morphometric features of the acetylcholine innervation in adult rat parietal cortex: an electron microscopic study in serial sections. J Comp Neurol 348:351–373.

Xiang Z, Huguenard JR, Prince DA (1998) Cholinergic switching within neocortical inhibitory networks. Science 281:985–988.

Zhang F, Gradinaru V, Adamantidis AR, Durand R, Airan RD, de Lecea L, Deisseroth K (2010) Optogenetic interrogation of neural circuits: technology for probing mammalian brain structures. Nat Protoc 5:439–456.